Translational PET Imaging of Spinal Cord Injury with the Serotonin Transporter Tracer [11C]AFM

Hanyi Fang[1,2], **Samantha Rossano**[1], **Xingxing Wang**[3], **Nabeel Nabulsi**[1], **Brian Kelley**[4], **Krista Fowles**[1], **Jim Ropchan**[1], **Stephen M. Strittmatter**[3], **Richard E. Carson**[1], **Yiyun Huang**[1]

[1]PET Center, Department of Radiology and Biomedical Imaging, Yale School of Medicine, New Haven, CT, USA

[2]Department of Nuclear Medicine, Union Hospital, Tongji Medical College, Huazhong University of Science and Technology, Wuhan, China

[3]Cellular Neuroscience, Neurodegeneration, and Repair Program, and Departments of Neurology and Neurobiology, Yale School of Medicine, New Haven, CT, USA

[4]Department of Neurosurgery, University of Pennsylvania, Philadelphia, PA, USA 2022

Abstract

Purpose: The descending raphespinal serotonin (5-HT) system contributes to neural activities required for locomotion. The presynaptic serotonin transporter (SERT) is a marker of 5-HT innervation. In this study, we explored the use of PET imaging with the SERT radioligand [11C]AFM as a biomarker of 5-HT axon damage after spinal cord injury (SCI) in a rodent model and its translation to imaging SCI in humans.

Procedures: PET imaging with [11C]AFM was performed in healthy rats under baseline and citalopram blocking conditions and a mid-thoracic transection rat model of SCI. The lumbar-to-cervical activity (L/C) ratio was calculated for the healthy and SCI animals to assess SERT binding decrease after SCI. Finally, translation of [11C]AFM PET was attempted to explore its potential to image SCI in humans.

Results: Intense uptake in the brain and intact spinal cord was observed at 30–60 min post-injection of [11C]AFM in healthy rats. About 65% of [11C]AFM uptake in the spinal cord was

blocked by citalopram. In the SCI rat model, the cervical uptake of [11C]AFM was similar to that in healthy rats, but the lumbar uptake was dramatically reduced, resulting in about half the L/C ratio in SCI rats compared to healthy rats. In contrast, [11C]AFM uptake in the human spinal cord showed no obvious decrease after treatment with citalopram. In the human subjects with SCI, decreases in [11C]AFM uptake were also not obvious in the section of spinal cord caudal to the injury point.

Conclusion: [11C]AFM PET imaging of SERT provides a useful preclinical method to non-invasively visualize the rodent spinal cord and detect SERT changes in SCI rodent models. However, there appears to be little detectable specific binding signal for [11C]AFM in the human spinal cord. An SERT tracer with higher affinity and lower non-specific binding signal is needed to image the spinal cord in humans and to assess the axonal status in SCI patients.

Keywords

PET imaging; Spinal cord injury; Serotonin transporter; [11C]AFM

Introduction

Traumatic spinal cord injury (SCI) is a disabling condition prevalent among the general population. According to the 2020 report of the National Spinal Cord Injury Statistical Center (NSCISC), there are over 17,000 new SCI cases reported each year and approximately 294,000 people living with SCI in the USA [1, 2]. SCI leads to temporary or permanent damage in the spinal cord's motor, sensory, and autonomic functions, which seriously affects the quality of life for these patients [3]. In the clinic, diagnosis and assessment of SCI rely primarily on physical and neurologic examinations through the observation of sensory and motor functions [4]. These observations are subjective and thus may introduce potential bias and inconsistencies. Traumatic SCI is a heterogeneous condition, and variability in outcome and treatment is influenced by many factors [5]. The availability of objective *in vivo* biomarkers may help to discern some of the heterogeneities in SCI patients. Furthermore, objective *in vivo* biomarkers may also be applied to the evaluation of patients who are unable to undergo routine examinations because of traumatic brain injury, multi-system trauma, or pharmacological sedation [5]. Therefore, an appropriate *in vivo* biomarker of SCI would enable a better correlation of functional status change in SCI patients to the recovery of axons and prediction of treatment outcomes.

Molecular imaging can provide powerful tools for combining *in vivo* biomarkers with anatomic localization. Medical imaging methods such as magnetic resonance imaging (MRI), computed tomography (CT), and positron emission tomography (PET) have been used for the non-invasive assessment of the structure and function of the human spinal cord [6]. MRI is currently considered the standard approach for the prognosis of acute SCI due to its high contrast and spatial resolution with accurate anatomical localization and multiple sequences for use. However, traumatic SCI leads to inflammation and disruption of the vascular supply, which can affect blood flow independent of neuronal activity and thus complicate the interpretation of MR signal changes [7]. A diverse set of radioligands has been evaluated in PET imaging studies for their ability to assess SCI [6]. These included the glucose metabolic tracer [18F]FDG [8–10], radioligands targeting the 18 kDa translocator

protein (TSPO) [11, 12], and myelin-specific radioligands [13, 14]. However, the uptake of [^{18}F]FDG is influenced by baseline glucose metabolic activities and inflammation, and the TSPO and myelin-targeted imaging biomarkers are indicators for the surrounding environment of the spinal cord after injury, but not of axonal changes.

Preclinical evidence has indicated that regeneration of serotonin (5-HT) axons caudal to the injury site is highly correlated with recovery of motor and sensory functions after SCI [15–18]. The descending raphespinal 5-HT system originates in the brainstem raphe nuclei and terminates in the superficial dorsal and ventral horns of the spinal cord [19]. The main function of 5-HT neurons in the brainstem is to promote locomotion by modulating the activity of spinal networks [20]. The serotonin transporter (SERT), located at the presynaptic plasma membrane of serotonergic neurons, is an important protein in the 5-HT system and regulates 5-HT homeostasis by re-absorbing extracellular 5-HT back into the cytoplasm [21, 22]. As such, SERT plays a critical role in mediating the function of the serotonergic system in locomotion [23]. When the spinal cord is injured, the serotonergic projections and other descending systems are severely damaged or completely cut off, resulting in 5-HT depletion, SERT dysregulation, and locomotor dysfunction [20]. SERT is reported to be highly expressed in the rodent spinal cord and its distribution parallels serotonergic innervation [19, 24]. Therefore, SERT could be a specific biomarker for the axonal status in the spinal cord, and SERT imaging may provide a useful non-invasive tool for the assessment of spinal cord injury.

Our previous studies showed that the SERT radioligand [^{11}C]AFM ([^{11}C]2-(2-(dimethylaminomethyl)phenylthio)-5-fluoromethylphenylamine) provides high specific binding signals in the brain [25, 26]. In a proof-of-concept study, we performed positron emission tomography (PET) imaging to characterize the specific binding of [^{11}C]AFM in the rat spinal cord and its ability to detect SERT changes in SCI model rats. Part of the results has been published previously in an abbreviated form [27]. In this report, we provide a detailed description and analysis of the preclinical study in rodents and report new PET imaging data from a translation study to image SERT in the spinal cord of healthy human subjects and patients with SCI.

Materials and Methods

Animal Models

All studies in animals were performed in accordance with protocols and policies approved by the Yale Institutional Animal Care and Use Committee. Female Sprague-Dawley rats (250–270 g, 11–12 weeks of age) were used. Mid-thoracic transection was applied to build the SCI model in rats ($n = 13$) using procedures reported by Wang *et al.* [27]. A laminectomy was conducted at the caudal portion of T6 and all of T7 spinal levels. The SCI model rats were imaged at 1 week after injury.

Human Subjects

Brain-only PET scans were performed in 4 male healthy volunteers, 28 ± 4.08 years (mean ± SD) of age with a range of 23 to 33 years, and BMI of 25.61 ± 2.61 (mean ± SD) with a

range of 22.57 to 28.95. Whole-body PET scans were performed in a healthy male volunteer (26-year-old, body mass index (BMI) = 21.98) and 2 male patients with SCI (age of 51 years and 47 years, respectively, with BMI of 35.26 and 25.82). SCI subject 1 had 30 years of chronic SCI with injury at the T4 level. SCI subject 2 had 12 years of chronic SCI with injury at the C5-C6 level. Both subjects were injured in motorcycle collisions and scored Grade A (complete impairment with no motor or sensory function left below the level of injury) on the American Spinal Injury Association (ASIA) Impairment Scale.

PET scans were performed under a protocol approved by the Human Investigation Committee (HIC, the local IRB) at Yale University School of Medicine and the Yale New Haven Hospital Radiation Safety Committee. The approval ID for this study was Yale HIC Protocol #0704002522. Study procedures were performed in accordance with federal guidelines and regulations of the USA for the protection of human research subjects contained in Title 45 Part 46 of the Code of Federal Regulations (45 CFR 46). Written informed consent was obtained from all subjects.

Evaluation of all subjects at the time of screening included a thorough neurological and psychiatric evaluation encompassing psychiatric history and assessment of treatment history, physical and neurological examination, electrocardiogram, blood and urine tests to establish that all participants were medically healthy. Urine samples were collected at the time of screening and on the day of the PET scan before the start of the scanning session and screened for drugs of abuse to ensure the drug-free status of all subjects. Evaluation of spinal cord-injured subjects also included examination of medical records at the time of injury so that a complete neurological examination at the time of entry into this study could be compared to the documented neurological examination at the time of injury to assess for neurological changes, severity, and spinal level of injury. Additionally, spinal imaging performed since the acute phase of injury was reviewed for anatomic correlation of all neurological findings.

PET Scanning Procedures

PET scans in rats (13 healthy controls and 13 SCI models) were performed as previously reported [27]. Rats were anesthetized using an RC2 Rodent Circuit manufactured by VetEquip with isoflurane inhalation (2.5% isoflurane/97.5% oxygen) under physiological temperatures (35.9 to 37.5 °C) in a temperature-regulated plexiglass cylinder. Heart and respiration rates were also monitored. The aperture of the high-resolution research tomograph (HRRT, Siemens Medical Systems) scanner was equipped with a custom-built insert to hold three cylinders symmetrically spaced for simultaneous imaging of three rats during each session. [11C]AFM was administered in sterile saline by tail vein injection with a dose of 50 ± 30 MBq per rat (injected mass = 0.12 ± 0.09 μg). After injection, dynamic PET images were acquired for 90 min. A subset of rats ($n = 4$) was imaged twice with [11C]AFM, under baseline condition, and after an injection of the selective serotonin transporter inhibitor citalopram (2 mg/kg in saline) via the tail vein 15 min prior to the second [11C]AFM PET scan to block specific binding.

Brain-only PET scans on the HRRT were performed as previously described [26]. [11C]AFM (dose: 717 ± 25 MBq, specific activity at the time of injection: 139 ± 39

GBq/μmol) was administered intravenously over 1 min by an automatic pump (Harvard PHD 22/2000; Harvard Apparatus, Holliston, MA, USA) and a 120min PET scan was acquired using the HRRT. The 4 healthy volunteers were imaged twice with [^{11}C]AFM, under baseline condition and after citalopram administration, respectively. Citalopram (20 mg) was administered orally 3 h prior to [^{11}C]AFM injection in the blocking scans.

Human participants in the whole-body PET scans were administered [^{11}C]AFM (activity doses for the baseline and blocking scans of the healthy control, and the two SCI subjects were 713 MBq, 746 MBq, 206 MBq, and 447 MBq, respectively) intravenously over 1 min by an automatic pump, and PET scans of 120min duration were acquired using a Biograph mCT PET/x-ray computed tomography (CT) scanner (Siemens Medical Solutions, Hoffman Estates, Knoxville, TN, USA). A CT scan was performed before each PET scan for attenuation correction. Both the whole-body baseline and blocking scans were performed on the healthy control, while only whole-body baseline scans were performed on the two SCI subjects. For the whole-body blocking scan in one healthy control, citalopram (20 mg) was administered orally 3 h prior to [^{11}C]AFM injection.

Image Analysis

The rat images acquired by the HRRT were reconstructed using a cluster-based list mode ordered subset expectation maximization (OSEM) algorithm (2 iterations, 30 subsets) with corrections for attenuation, random, scatter, and deadtime. Regions of interest (ROIs) of rats were drawn manually in the cervical and lumbar regions of the spinal cord with the shape of thin rectangles oriented axially along the spinal cord manually placed around the highest uptake areas in the cervical and lumbar regions, respectively.

The reconstruction, image registration, ROIs, kinetic modeling, and parametric imaging of brain-only human images acquired by the HRRT were performed as described previously [26]. For the brain-only [^{11}C]AFM PET scans, the regional volume of distribution (V_T) from both the baseline and citalopram blocking scans was estimated using the multilinear analysis-1 (MA1) method [26] and used to estimate citalopram occupancy [28].

The whole-body (multi-bed) dynamic PET data acquired on the mCT were reconstructed with the OSEM algorithm with point spread function correction using time-of-flight measurements. Frame timing was 5×108 s, 5×216 s, 5×432 s, and 3×1080 s. ROIs of human whole-body PET scans were drawn manually for the striatum, cerebellum, and spinal cord at the cervical and lumbar regions. The shape of ROIs was round, and average ROI volumes of the spinal cord at the cervical and lumbar regions were 65.77 ± 29.47 cm^3 and 236.95 ± 85.9 cm^3, respectively, across the four scans in three human subjects.

Statistical Analysis

Data analyses were conducted using GraphPad Prism 6.0 (GraphPad Software, San Diego, CA, USA). Results were expressed as mean ± standard deviation of the mean (mean ± SD). The independent samples Mann–Whitney U test was used to analyze the differences of PET parameters (SUV$_{mean}$ and the lumbar to cervical uptake ratio) between the group of healthy rats undergoing both the baseline and citalopram blocking scans ($n = 4$) and the groups of healthy and SCI model rats ($n = 13$).

Results

[^{11}C]AFM PET Imaging in Rats

Note that part of the results in rats has been described previously [27], while more details are presented here. For the baseline scan, high uptake was found in the brain and spinal cord at 30–60 min post-injection (Fig. 1a). Pretreatment of the rats with citalopram led to markedly decreased uptake of [^{11}C]AFM both in the brain and spinal cord (Fig. 1b). In the SCI model rats generated by mid-thoracic transection and imaged at 1 week after injury, [^{11}C]AFM uptake was reduced in the lumbar section below the injury point, in comparison to that in the healthy animals, while uptake in the cervical section was preserved (Fig. 1c).

Time-activity Curves in Rats

Time-activity curves (TACs) were generated for ROIs in the brain, and cervical and lumbar sections of the spinal cord. In the baseline scans of healthy rats, as expected, a much higher uptake of [^{11}C]AFM was seen in the brain (Fig. 2a), and similar levels of uptake in the cervical and lumbar regions of the spinal cord were displayed (Fig. 2b, c). Citalopram blocking reduced uptake in the brain, cervical, and lumbar ROIs to the same levels, indicating that non-specific binding of [^{11}C]AFM was similar in both the brain and spinal cord (Fig. 2a–c).

In the baseline scans of healthy rats, the mean standard uptake values (SUV$_{mean}$) of [^{11}C]AFM from 30 to 60 min post-injection was 1.80 ± 0.10 in the cervical region of the spinal cord and 1.95 ± 0.27 in the lumbar region (Fig. 2d). The lumbar-to-cervical (L/C) uptake ratio was 1.08 ± 0.12 (Fig. 2e). In the blocking scans with citalopram, [^{11}C]AFM SUV$_{mean}$ was 0.64 ± 0.12 and 0.66 ± 0.16, respectively, for the cervical and lumbar regions, a reduction of about 65% compared to the baseline scans (Fig. 2d–e). The L/C uptake ratio was 1.03 ± 0.19 in the blocking scans, similar to that in the baseline scans (Fig. 2e). These results demonstrated that a large percentage of [^{11}C]AFM binding in the spinal cord was specific to SERT, and there was no difference in [^{11}C]AFM specific binding between the cervical and lumbar regions of the spinal cord.

In SCI model rats, the lumbar signal was significantly reduced compared to the cervical signal with an L/C uptake ratio of 0.46 ± 0.11 ($P < 0.001$), less than half of that in the healthy control rats (Fig. 2d, e).

[^{11}C]AFM PET Imaging in Human

There were two parts of PET imaging with [^{11}C]AFM in human subjects: The first part was brain-only imaging in four healthy subjects under baseline and citalopram blocking conditions to measure the specific binding component of [^{11}C]AFM in the brain, and the second part was whole-body imaging with [^{11}C]AFM in one healthy subject and two patients with SCI to explore the feasibility of SERT imaging in the spinal cord.

[^{11}C]AFM PET images from the brain-only scans under baseline and citalopram blocking conditions in a healthy human subject are shown in Fig. 3. As reported in our previous study [26], high radioactivity accumulation was seen in the thalamus, putamen, and caudate, and

lower in the cerebellum in the baseline scan, while uptake in all brain regions decreased after pretreatment with citalopram (20 mg, p.o.).

Shown in Fig. 4 are PET SUV images of [^{11}C]AFM from one healthy and two SCI subjects. In the healthy subject, high uptake was seen in the brain and lungs and low uptake in the spinal cord (Fig. 4a). Pretreatment with citalopram resulted in visible reductions of [^{11}C]AFM uptake in the brain and lungs, but not in the spinal cord (Fig. 4b). In the two SCI subjects, no visible difference in radioactivity uptake was observed between the cervical and lumbar sections of the spinal cord (Fig. 4c, d).

Time-activity Curves in Human and Quantification of Imaging Data

Regional time-activity curves from one healthy subject undergoing brain-only PET scans are shown in Fig. 5. In the baseline scan, [^{11}C]AFM uptake pattern in the brain was consistent with that of our previous study [25, 26]. Higher uptake was seen in the thalamus and lower in the cerebellum, with both showing a peak followed by appreciable wash-out (Fig. 5a). In the blocking scan, [^{11}C]AFM uptake in all brain regions cleared quickly after the initial uptake phase and reached similar levels after 30min post-injection (Fig. 5b).

The regional volume of distribution (V_T) derived from MA1 analysis is listed in Table 1 for the four subjects in the brain-only baseline-blocking study on the HRRT. Regional V_T values of thalamus, putamen, caudate, amygdala, hippocampus, and cingulum were significantly reduced in the citalopram blocking scans ($P < 0.01$). Based on occupancy plots derived from regional V_T values in the baseline and blocking scans, pretreatment with citalopram resulted in 94.28 ± 2.48 % SERT occupancy in the brain (Fig. 5c).

PET data from whole-body scans with [^{11}C]AFM on the mCT are presented in Fig. 6. The uptake pattern in the thalamus and cerebellum was similar to that of the subjects undergoing brain-only PET scans (Fig. 6a, b, compared with Fig. 5a, b). Time-activity curves for the cervical and lumbar regions of the spinal cord are shown in Fig. 6c, d. For the analysis of uptake in the spinal cord, we calculated the mean SUV from 30 to 60 min post-injection ($SUV_{mean, 30-60}$) for the cervical and lumbar region and their ratio (L/C ratio). In the one healthy subject undergoing whole-body baseline and citalopram blocking scans, $SUV_{mean, 30-60}$ was 0.64 and 0.51, respectively, for the cervical and lumbar sections in the baseline scan, and 0.96 and 0.94 in the citalopram blocking scan (Fig. 6e). The L/C ratios were 0.79 and 0.98, respectively, in the baseline and blocking scans (Fig. 6g). For the SCI_1 subject, the $SUV_{mean, 30-60}$ was 0.64 and 0.47, respectively, for the cervical and lumbar sections with an L/C ratio of 0.73, both the $SUV_{mean, 30-60}$ and the L/C ratio were similar to those of the healthy control (Fig. 6c, d, f, g). For the SCI_2 subject, the $SUV_{mean, 30-60}$ was 0.27 and 0.42, respectively, with an L/C ratio of 1.56 (Fig. 6c, d, f, g). In the human spinal cord, SERT-specific binding of [^{11}C]AFM cannot be definitively demonstrated because citalopram showed little, if any, detectable blocking effect in the spinal cord of the healthy subject (Fig. 6e).

Discussion

In this study, we demonstrated that SERT could be a biomarker for spinal cord injury and [11C]AFM PET imaging of SERT used to assess SCI in rats. The blocking study with citalopram showed a 65% decrease in [11C]AFM uptake, indicating that its binding was specific to SERT in the spinal cord. Furthermore, non-specific binding of [11C]AFM appeared to be the same in the brain and spinal cord in rats, as citalopram reduced uptake in both to similar levels. In the SCI model rats with mid-thoracic transection, [11C]AFM uptake in the lumbar region was reduced significantly, resulting in an L/C ratio of 0.46 vs. unity in the healthy controls, indicating that [11C]AFM was able to detect decreased SERT concentrations in the lumbar section after SCI.

These imaging results are in accordance with the changes of SERT after SCI in rats. A quantitative autoradiography study detected a significant decrease in SERT at the lumbar level 2 weeks after SCI [29]. An immunohistochemistry study performed by Kong *et al.* reported that SERT rapidly diminished by 2 days after SCI and completely disappeared after 3 weeks at the injury sites [30]. As previously reported by Wang *et al.* [27], postmortem histological examination of SERT axon length showed a lumbar (below the transection level) to midthoracic (above the transection level) ratio of about 0.5 in SCI rats, which was similar to the L/C uptake ratio obtained through PET imaging, indicating a good correlation between histology and PET imaging findings in the spinal cord of SCI rats.

[11C]AFM PET imaging has been successfully used for the visualization and quantification of brain SERT *in vivo* [25, 26, 31]. The cerebellum, an SERT-poor region, was used as a reference region [32–34]. The region-to-cerebellum ratio reached 6 for the thalamus, hypothalamus, and frontal cortex at 60 min post-injection, indicating high specific binding of [11C]AFM in these SERT-rich brain regions in rats [25]. In the human brain, [11C]AFM V_T and binding potential (BP_{ND}) values in the thalamus of healthy human subjects were 40.3 ± 0.21 and 2.81 ± 0.12 ($n = 10$), respectively, as estimated by the MA1 kinetic modeling method [26]. Although previous studies reported negligible SERT density in the human cerebellum [32–34], [11C]AFM V_T in the cerebellum was reduced by 15% to 8.19 ± 1.09 by citalopram pretreatment, from 9.70 ± 0.85 ($n = 4$) in the baseline studies in humans, suggesting that cerebellum may not be an ideal reference region for SERT in human studies [26, 35].

Encouraged by the ability of [11C]AFM to image the intact spinal cord with quantifiable specific binding signals in healthy rats and to detect decreased SERT density in regions caudal to the injury site [27], we carried out a feasibility study of imaging SERT in the human spinal cord with [11C] AFM. Although uptake in the brain and lungs was blocked by pretreatment with citalopram and the TACs for brain regions of both baseline and blocking scans showed a similar shape to that in our previous study of [11C]AFM imaging in the human brain [25, 26], [11C]AFM uptake in the human spinal cord was not reduced by pretreatment with citalopram, indicating negligible specific binding of [11C]AFM in the spinal cord. There was actually higher spinal cord uptake of [11C]AFM in the human blocking study than that of the baseline scan at an early time in the scan. Higher initial uptake in the brain has been observed in blocking scans of SERT tracers (Fig. 5a, b). This

is due to the blockade of binding sites in the periphery (e.g., lungs); hence, more [^{11}C]AFM is available to enter the brain (and spinal cord), leading to higher initial radioactivity concentrations in the brain and spinal cord. The radioactivity then cleared rapidly due to blockade of the binding sites in the brain. Therefore, it appears that [^{11}C]AFM PET is not feasible to image spinal cord injury in humans.

The most likely explanation for the inability of [^{11}C]AFM to image SCI in humans is a dramatically reduced SERT density in the human spinal cord compared to that in rodents. As it is well known, the PET imaging signal provided by a radioligand, as defined by the non-displaceable binding potential (BP_{ND}), is dependent on the density of the imaging target ($B_{\max}$), the affinity (K_{D}) of the radioligand for the target, and the non-specific binding level of the radioligand [36]. Since the K_{D} and non-specific binding level of [^{11}C]AFM (the latter was supported by citalopram blocking scans in rodents and humans in the current study) is assumed to be the same in both the brain and spinal cord, dramatically diminished SERT $B_{\max}$ in the human spinal cord would result in a non-detectable level of the specific binding signal. Based on this analysis, successful PET imaging of SERT in the human spinal cord will require the development of radioligands with reliably detectable specific binding signals, i.e., with higher affinity and/or lower non-specific binding level than [^{11}C]AFM.

PET imaging of SERT in SCI, as reported in our current study, provides a valuable tool to directly assess axonal damage in SCI and status change during treatment and recovery because of the close association between 5-HT innervation and motor/sensory function in the spinal cord. Obviously, SCI is a heterogeneous disease that impacts many biological pathways. PET imaging with radiotracers for different biomarkers can be used to investigate the multi-faceted pathways involved in this disease and provide tools and insights for its diagnosis and therapy.

There are some limitations to this study. Since each human SCI case is unique in position and severity of the injury, we were unable to fully match them with those in the experimental animal model. As a result, the animal models used were female rats with thoracic injuries, while the SCI subjects were two males with injuries at the C5-C6 and T4 levels. Therefore, any potential effects of sex and injury level will require further investigation in future studies.

Conclusion

In this study, we demonstrated the ability of [^{11}C]AFM to provide SERT-specific binding signals in the rodent spinal cord and to detect SERT changes in SCI models. Therefore, PET imaging with [^{11}C]AFM provides a useful preclinical tool for the non-invasive visualization and quantification of SERT in rodent models of spinal cord injury. Although [^{11}C]AFM displays limited detectible specific binding signals in the human spinal cord, continued effort in this area may eventually furnish a higher affinity SERT tracer suitable for clinical PET imaging of the human spinal cord to assess the axonal status in SCI in association with motor and sensory functions.

References

1. Jain NB, Ayers GD, Peterson EN et al. (2015) Traumatic spinal cord injury in the United States, 1993–2012. JAMA 313:2236–2243 [PubMed: 26057284]

2. Lasfargues JE, Custis D, Morrone F, Carswell J, Nguyen T (1995) A model for estimating spinal cord injury prevalence in the United States. Paraplegia 33:62–68 [PubMed: 7753569]

3. Fakhoury M (2015) Spinal cord injury: overview of experimental approaches used to restore locomotor activity. Rev Neurosci 26:397–405 [PubMed: 25870961]

4. Eckert MJ, Martin MJ (2017) Trauma: spinal cord injury. Surg Clin North Am 97:1031–1045 [PubMed: 28958356]

5. Badhiwala JH, Wilson JR, Kwon BK, Casha S, Fehlings MG (2018) A review of clinical trials in spinal cord injury including biomarkers. J Neurotrauma 35:1906–1917 [PubMed: 29888678]

6. Stroman PW, Wheeler-Kingshott C, Bacon M et al. (2014) The current state-of-the-art of spinal cord imaging: methods. Neuroimage 84:1070–1081 [PubMed: 23685159]

7. Harel NY, Strittmatter SM (2008) Functional MRI and other non-invasive imaging technologies: providing visual biomarkers for spinal cord structure and function after injury. Exp Neurol 211:324–328 [PubMed: 18396280]

8. Tewarie RDSN, Yu J, Seidel J, et al. (2010) Positron emission tomography for serial imaging of the contused adult rat spinal cord. Molecular Imaging 9:108–116 [PubMed: 20236603]

9. von Leden RE, Selwyn RG, Jaiswal S, Wilson CM, Khayrullina G, Byrnes KR (2016) ^{18}F-FDG-PET imaging of rat spinal cord demonstrates altered glucose uptake acutely after contusion injury. Neurosci Lett 621:126–132 [PubMed: 27084688]

10. von Leden RE, Moritz KE, Bermudez S et al. (2019) Aging alters glucose uptake in the naive and injured rodent spinal cord. Neurosci Lett 690:23–28 [PubMed: 30296507]

11. Imamoto N, Momosaki S, Fujita M et al. (2013) [^{11}C]PK11195 PET imaging of spinal glial activation after nerve injury in rats. Neuroimage 79:121–128 [PubMed: 23611861]

12. Tremoleda JL, Thau-Zuchman O, Davies M et al. (2016) In vivo PET imaging of the neuroinflammatory response in rat spinal cord injury using the TSPO tracer [^{18}F]GE-180 and effect of docosahexaenoic acid. Eur J Nucl Med Mol Imaging 43:1710–1722 [PubMed: 27154521]

13. Wu C, Eck B, Zhang S et al. (2017) Discovery of 1,2,3-triazole derivatives for multimodality PET/CT/cryoimaging of myelination in the central nervous system. J Med Chem 60:987–999 [PubMed: 28107629]

14. Tiwari AD, Zhu J, You J et al. (2019) Novel ^{18}F-labeled radioligands for positron emission tomography imaging of myelination in the central nervous system. J Med Chem 62:4902–4914 [PubMed: 31042384]

15. Saruhashi Y, Matsusue Y, Fujimiya M (2009) The recovery of 5-HT transporter and 5-HT immunoreactivity in injured rat spinal cord. Arch Orthop Trauma Surg 129:1279–1285 [PubMed: 18825396]

16. Engesser-Cesar C, Ichiyama RM, Nefas AL et al. (2007) Wheel running following spinal cord injury improves locomotor recovery and stimulates serotonergic fiber growth. Eur J Neurosci 25:1931–1939 [PubMed: 17439482]

17. Hashimoto T, Fukuda N (1991) Contribution of serotonin neurons to the functional recovery after spinal cord injury in rats. Brain Res 539:263–270 [PubMed: 1829012]

18. Saruhashi Y, Young W, Perkins R (1996) The recovery of 5-HT immunoreactivity in lumbosacral spinal cord and locomotor function after thoracic hemisection. Exp Neurol 139:203–213 [PubMed: 8654523]

19. Sur C, Betz H, Schloss P (1996) Localization of the serotonin transporter in rat spinal cord. Eur J Neurosci 8:2753–2757 [PubMed: 8996825]

20. Ghosh M, Pearse DD (2014) The role of the serotonergic system in locomotor recovery after spinal cord injury. Front Neural Circuits 8:151 [PubMed: 25709569]

21. Murphy DL, Lerner A, Rudnick G, Lesch KP (2004) Serotonin transporter: gene, genetic disorders, and pharmacogenetics. Mol Interv 4:109–123 [PubMed: 15087484]

22. Hains BC, Everhart AW, Fullwood SD, Hulsebosch CE (2002) Changes in serotonin, serotonin transporter expression and serotonin denervation supersensitivity: involvement in chronic central pain after spinal hemisection in the rat. Exp Neurol 175:347–362 [PubMed: 12061865]

23. Husch A, Van Patten GN, Hong DN, Scaperotti MM, Cramer N, Harris-Warrick RM (2012) Spinal cord injury induces serotonin supersensitivity without increasing intrinsic excitability of mouse V2a interneurons. J Neurosci 32:13145–13154 [PubMed: 22993431]

24. Bowker RM, Westlund KN, Coulter JD (1981) Origins of serotonergic projections to the spinal cord in rat: an immunocytochemical-retrograde transport study. Brain Res 226:187–199 [PubMed: 7028211]

25. Huang Y, Hwang DR, Bae SA et al. (2004) A new positron emission tomography imaging agent for the serotonin transporter: synthesis, pharmacological characterization, and kinetic analysis of [^{11}C]2-[2-(dimethylaminomethyl)phenylthio]-5-fluoromethylphenylamine ([^{11}C]AFM). Nucl Med Biol 31:543–556 [PubMed: 15219271]

26. Naganawa M, Nabulsi N, Planeta B et al. (2013) Tracer kinetic modeling of [^{11}C]AFM, a new PET imaging agent for the serotonin transporter. J Cereb Blood Flow Metab 33:1886–1896 [PubMed: 23921898]

27. Wang X, Duffy P, McGee AW et al. (2011) Recovery from chronic spinal cord contusion after Nogo receptor intervention. Ann Neurol 70:805–821 [PubMed: 22162062]

28. Cunningham VJ, Rabiner EA, Slifstein M, Laruelle M, Gunn RN (2010) Measuring drug occupancy in the absence of a reference region: the Lassen plot re-visited. J Cereb Blood Flow Metab 30:46–50 [PubMed: 19738632]

29. Rojo ML, Rodriguez-Gaztelumendi A, Pazos A, Diaz A (2012) Differential adaptive changes on serotonin and noradrenaline transporters in a rat model of peripheral neuropathic pain. Neurosci Lett 515:181–186 [PubMed: 22480692]

30. Kong XY, Wienecke J, Chen M, Hultborn H, Zhang M (2011) The time course of serotonin 2A receptor expression after spinal transection of rats: an immunohistochemical study. Neuroscience 177:114–126 [PubMed: 21211552]

31. Murrough JW, Huang Y, Hu J et al. (2011) Reduced amygdala serotonin transporter binding in posttraumatic stress disorder. Biol Psychiatry 70:1033–1038 [PubMed: 21855859]

32. Laruelle M, Vanisberg MA, Maloteaux JM (1988) Regional and subcellular localization in human brain of [^{3}H]paroxetine binding, a marker of serotonin uptake sites. Biol Psychiatry 24:299–309 [PubMed: 2969755]

33. Cortes R, Soriano E, Pazos A, Probst A, Palacios JM (1988) Autoradiography of antidepressant binding sites in the human brain: localization using [^{3}H]imipramine and [^{3}H]paroxetine. Neuroscience 27:473–496 [PubMed: 2975361]

34. Backstrom I, Bergstrom M, Marcusson J (1989) High affinity [^{3}H]paroxetine binding to serotonin uptake sites in human brain tissue. Brain Res 486:261–268 [PubMed: 2525060]

35. Kish SJ, Furukawa Y, Chang LJ et al. (2005) Regional distribution of serotonin transporter protein in postmortem human brain: is the cerebellum a SERT-free brain region? Nucl Med Biol 32:123–128 [PubMed: 15721757]

36. Innis RB, Cunningham VJ, Delforge J et al. (2007) Consensus nomenclature for in vivo imaging of reversibly binding radioligands. J Cereb Blood Flow Metab 27:1533–1539 [PubMed: 17519979]
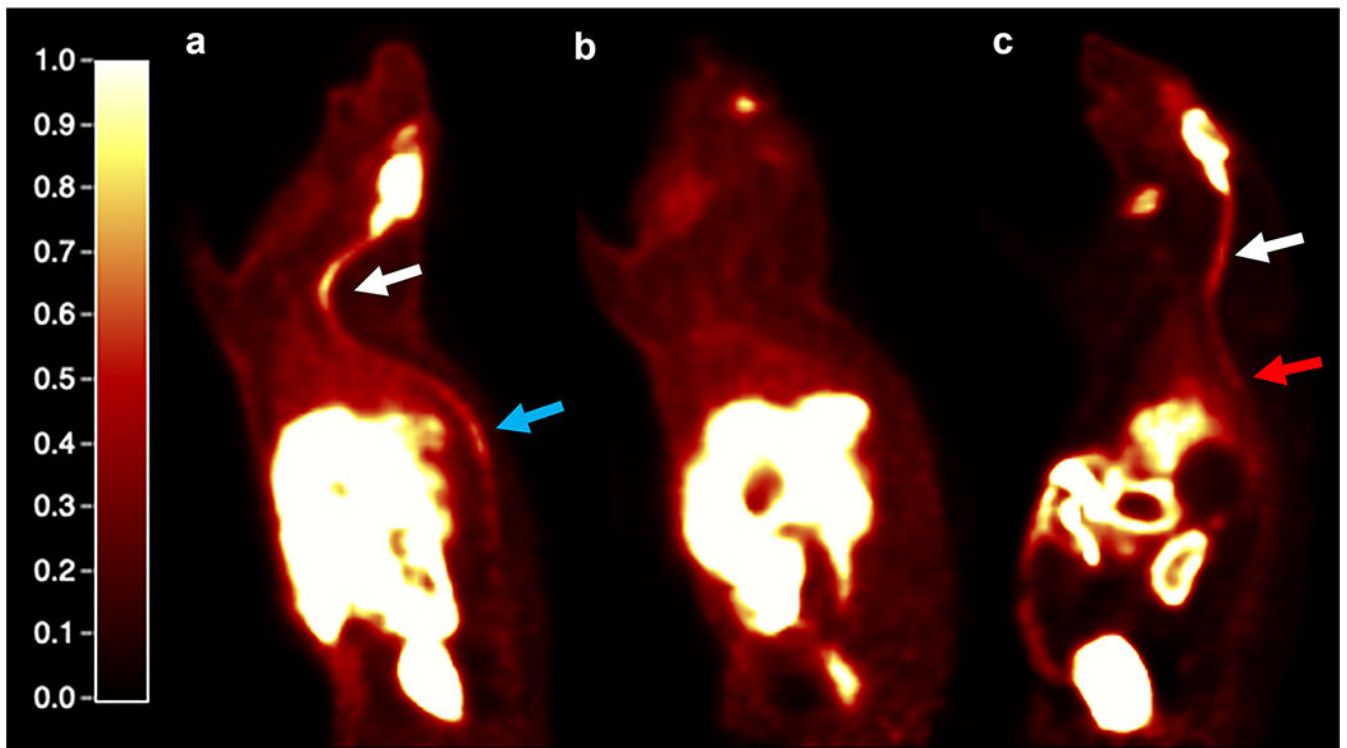
Fig. 1.
[^{11}C]AFM PET images at 30–60 min post-injection from the baseline scan of (**a**) a healthy rat, (**b**) after treatment with citalopram, and (**c**) in an SCI rat. The white arrows indicate the cervical ROI, blue arrow the lumbar ROI, and red arrow the injury region. The SUV color scale ranged from 0 to 1. Images were reprocessed from those of the animals imaged in [27].
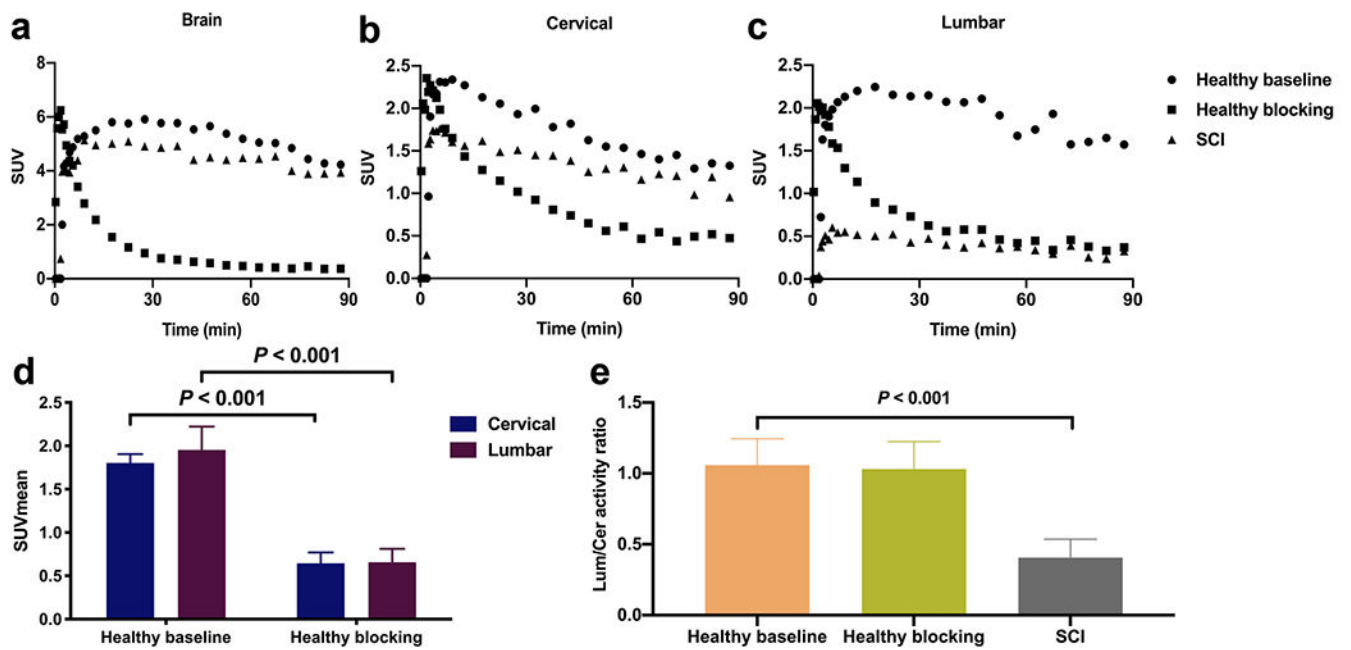
Fig. 2.

[^{11}C]AFM PET imaging results in rats: representative TACs for the brain (**a**), and cervical (**b**) and lumbar (**c**) sections of the spinal cord from the baseline and citalopram blocking scans in a healthy rat, and baseline scan in an SCI rat; (**d**) SUV$_{mean}$ for the cervical and lumbar sections of the spinal cord from the baseline and citalopram blocking scans in a healthy rat, summed from 30 to 60 min post-injection (mean ± SD, $n = 4$); (**e**) The lumbar-to-cervical activity ratio from the baseline and citalopram blocking scans in healthy rats, and baseline scans in SCI rats (mean ± SD, $n = 13$).
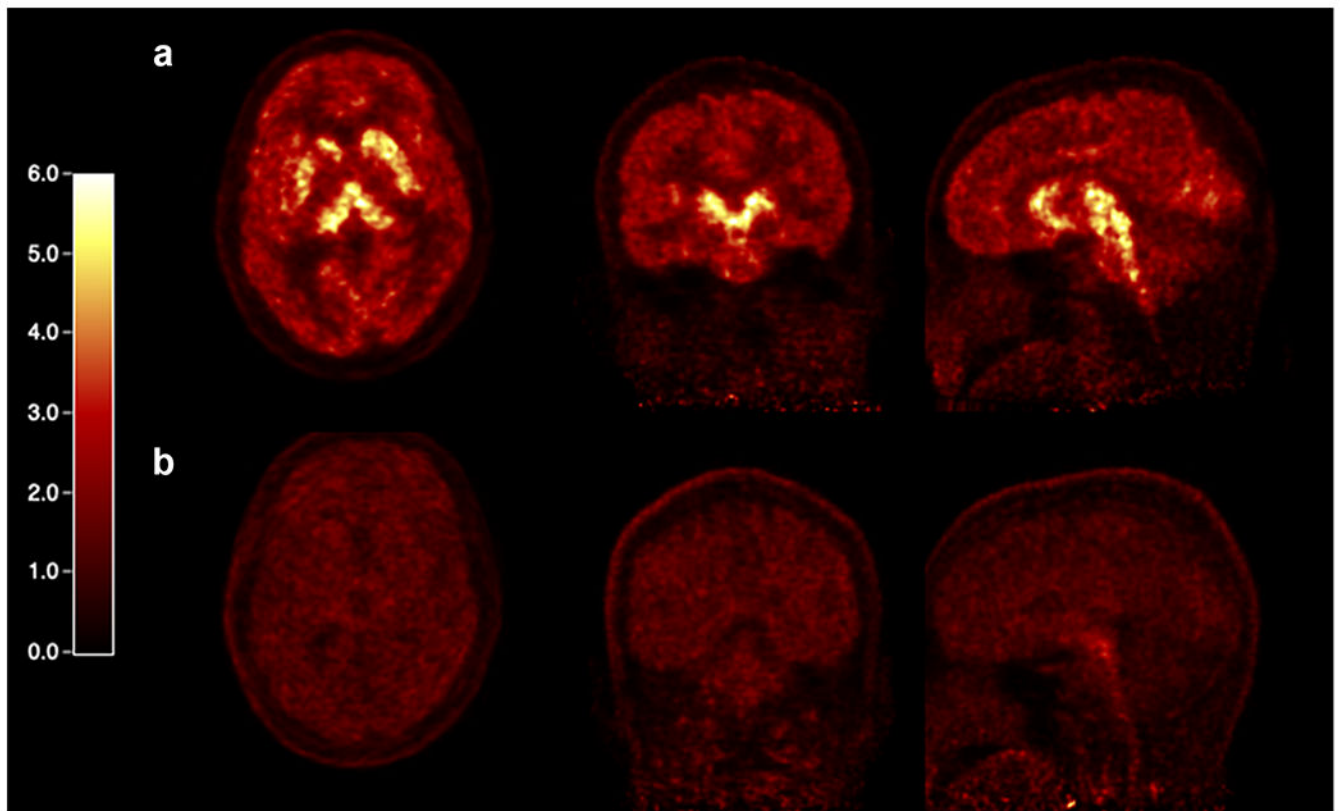
Fig. 3.
PET SUV images of [^{11}C]AFM in the brain summed from 40 to 60 min post-injection of (**a**) the baseline scan and (**b**) citalopram blocking scan of a healthy human subject.
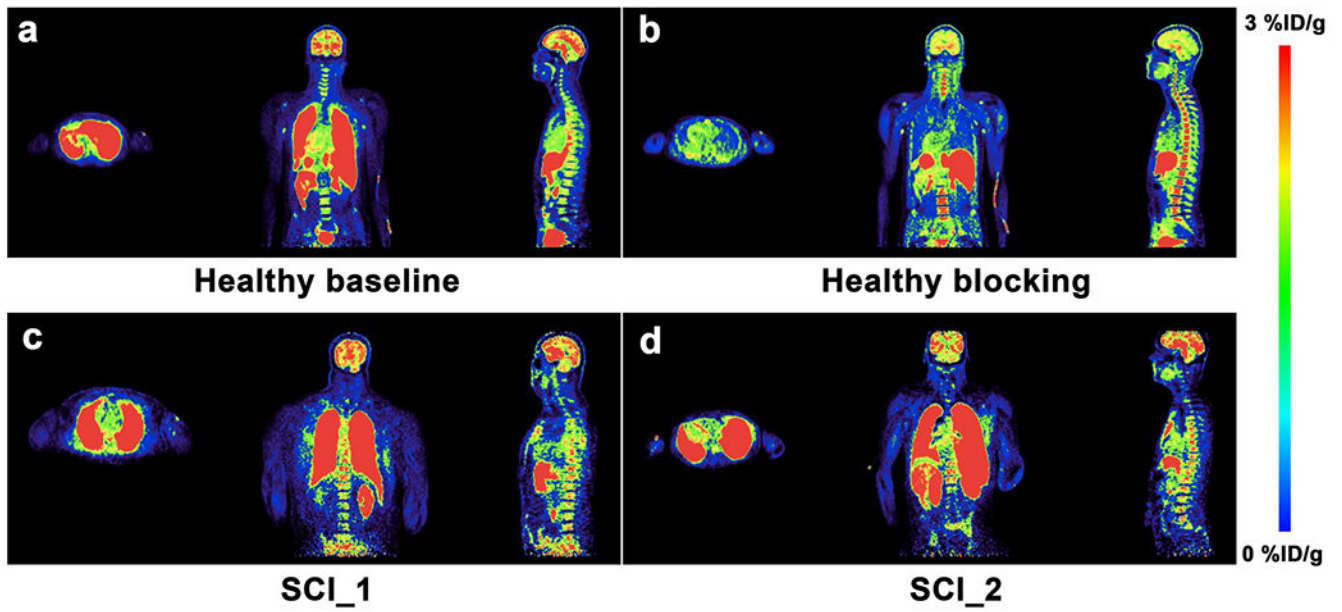
Fig. 4.
PET SUV images of [^{11}C]AFM summed from 30 to 60 min post-injection in (**a**) the baseline scan and (**b**) citalopram blocking scan of a healthy human subject, as well as (**c** and **d**) two different SCI subjects. An obvious blockade of [^{11}C]AFM uptake is seen in the brain and lungs of the healthy subject. The SUV color scale ranges from 0 to 3 % ID/g.
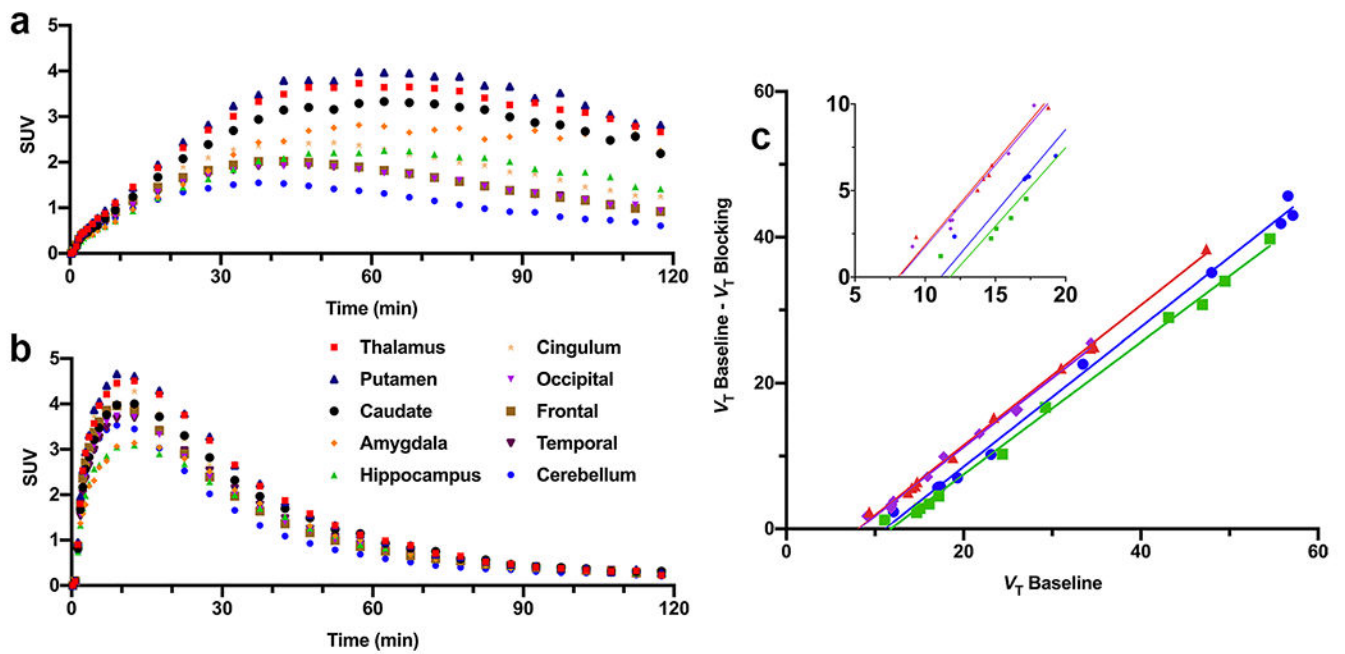
Fig. 5.
Brain regional TACs of [^{11}C]AFM from (**a**) the baseline scan and (**b**) citalopram blocking scan of a healthy human subject, and (**c**) occupancy plots from the citalopram blocking scans in four different subjects.
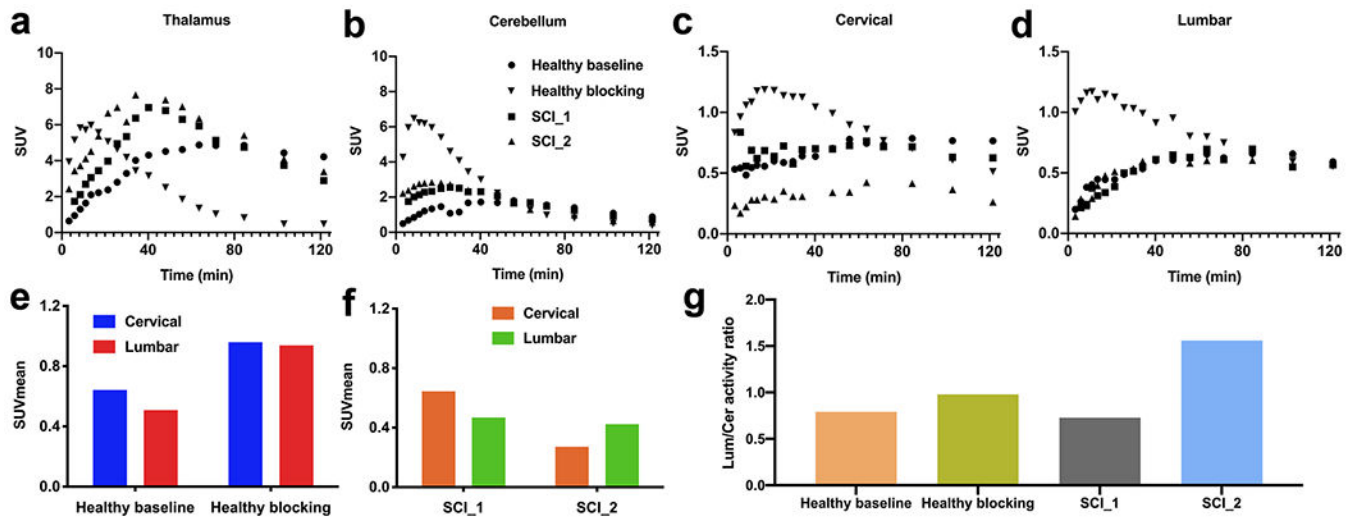
Fig. 6.

[^{11}C]AFM PET study in human subjects. The thalamus (**a**), cerebellum (**b**), cervical (**c**), and lumbar (**d**) TACs from the baseline and citalopram blocking scans in a healthy subject, and baseline scans in two SCI subjects. The cervical and lumbar SUV$_{mean}$ from 30 to 60 min post-injection for the spinal cord in the baseline and blocking scans of a healthy subject (**e**) and two human SCI subjects (**f**). (**g**) Lumbar-to-cervical activity ratio in two SCI subjects, and from the baseline and citalopram blocking studies in a healthy subject.

Table 1.

Regional volume of distribution (V_T, ml/cm^3) from the baseline and citalopram blocking scans ($n = 4$ each) in the brain-only [^{11}C]AFM PET study, estimated by the multilinear analysis-1 (MAI) method. Data are mean ± SD.

Regions	Baseline	Blocking
Thalamus	35.57 ± 8.57	11.86 ± 2.07
Putamen	36.20 ± 8.57	12.13 ± 2.22
Caudate	30.55 ± 6.84	10.83 ± 1.88
Amygdala	43.00 ± 9.15	10.54 ± 1.66
Hippocampus	21.83 ± 4.27	9.54 ± 1.53
Cingulate cortex	18.32 ± 2.04	10.58 ± 1.72
Occipital lobe	13.66 ± 1.14	10.06 ± 1.13
Frontal lobe	14.37 ± 1.31	9.97 ± 1.30
Temporal lobe	14.11 ± 1.25	10.02 ± 1.31
Cerebellum	9.70 ± 0.85	8.19 ± 1.09